Polyimide based all-organic sodium ion battery

Article *in* Journal of Materials Chemistry A · April 2015

DOI: 10.1039/C5TA02043C

CITATIONS
120

READS
772

5 authors, including:

Harish Banda
Massachusetts Institute of Technology
16 PUBLICATIONS **698** CITATIONS
SEE PROFILE

Dijo Damien
Christ College, Irinjalakuda
20 PUBLICATIONS **1,214** CITATIONS
SEE PROFILE

Kalaivanan Nagarajan
University of Strasbourg
33 PUBLICATIONS **1,509** CITATIONS
SEE PROFILE

Mahesh Hariharan
Indian Institute Of Science Education and Research, Thiruvananthapuram
112 PUBLICATIONS **2,716** CITATIONS
SEE PROFILE

Journal of Materials Chemistry A

PAPER

View Article Online
View Journal

Cite this: DOI: 10.1039/c5ta02043c

A polyimide based all-organic sodium ion battery†

Harish Banda,[ab] Dijo Damien,[ab] Kalaivanan Nagarajan,[b] Mahesh Hariharan[b] and Manikoth M. Shaijumon*[a]

Received 19th March 2015
Accepted 7th April 2015

DOI: 10.1039/c5ta02043c

www.rsc.org/MaterialsA

Developing new approaches to improve the performance of organic electrodes for rechargeable sodium batteries is important. Here, we report studies on *N,N′*-diamino-3,4,9,10-perylenetetracarboxylic polyimide (PI) as a novel cathode for a sodium battery and demonstrate an all-organic sodium ion battery using this polyimide as the cathode and disodium terephthalate (NaTP) (pre-sodiated) as the anode. The synthesised PI exhibits excellent electrochemical properties, when studied as the cathode for sodium batteries, with a reversible capacity of 126 mA h g^{-1} along with good capacity retention and rate capability, in the voltage range of 1.5 to 3.5 V *vs.* Na^+/Na. The all-organic sodium ion full cell delivered an initial capacity of 73 mA h g^{-1}, with an average cell voltage of 1.35 V. The attractive electrochemical performance combined with the design flexibility of a PTCDA based PI material, offer new possibilities for the development of efficient all-organic sodium ion batteries.

1. Introduction

Lithium ion batteries (LIBs) have been at the forefront of energy storage technologies for a range of portable device applications over the past couple of decades and have been recently looked at to meet the on-board energy requirements in vehicular applications. However, with the recent concerns on the availability of lithium and the high cost associated with the bulk production of LIBs, sodium ion batteries (SIBs) have been regarded as a promising alternative to LIBs, particularly for large-scale applications.[1–3] Recently, there has been great interest in developing advanced electrode materials for SIBs, and a large number of materials involving transition metals have been proposed as cathodes, similar to those explored for LIBs.[4–8] While high voltage and good cyclability have been the thriving factors for these materials, the associated environmental concerns and their higher production costs question the long term reliance on these inorganic materials used in SIBs for large-scale applications. Organic materials, owing to their abundance, design flexibility and environmental benignancy, have lately enjoyed a renewed interest as electrodes in rechargeable lithium batteries.[9–11] Various reports demonstrating high lithium storage capacities, possible multi-electron reactions and tuneable redox potentials have appeared recently in the literature.[12–20] The mechanism of lithiation/de-lithiation in organic compounds involves a reversible redox reaction of the respective organic functional groups such as keto, carboxylate, anhydride, and so on along with the insertion/de-insertion of Li^+ ions at the respective redox centres. The enolates thus formed are stabilized by extended conjugation in the aromatic rings.

One of the key challenges for organic electrode materials is the dissolution of the active material into electrolytes during charge–discharge cycling, resulting in poor cycling performances.[21,22] Several strategies have been suggested to resolve the dissolution issue, such as the non-covalent or covalent attachment of redox molecules to substrates, polymerization of the active compound, optimization of the molecular structure, and the use of solid electrolytes.[21,23–28] Polymerisation of the active compound is particularly interesting owing to its versatility and the added advantages of improved thermal stability and increased kinetics of electron transfer through polymer chains.[21,23]

Unfortunately, the progress on organic electrode materials on the sodium front has been limited and only very recently, the work on organic based electrodes for SIBs did gain momentum.[29–34] Polyimides, with their good thermal stability and electronic conductivity,[24] undergo reversible sodiation/de-sodiation processes alongside the redox conversion of the imide functionality to an enolate. Recent reports on 1,4,5,8-naphthalenetetracarboxylic dianhydride (NTCDA) derived polyimides as cathodes for SIBs show good cycling stability and power capability but offer lower voltages.[35,36] 3,4,9,10-Perylenetetracarboxylic dianhydride (PTCDA) derived polyimides offer higher reduction potentials and in turn higher energy densities.[37] Zhang *et al.*, demonstrated various diamines as polymerising agents for PTCDA.[38] Ethylene diamine, 1,3-propylene

[a]*School of Physics, Indian Institute of Science Education and Research, Thiruvananthapuram, CET Campus, Sreekaryam, Thiruvananthapuram, Kerala, 695016, India. E-mail: shaiju@iisertvm.ac.in*

[b]*School of Chemistry, Indian Institute of Science Education and Research, Thiruvananthapuram, CET Campus, Sreekaryam, Thiruvananthapuram, Kerala, 695016, India*

† Electronic supplementary information (ESI) available: Characterization through FT-IR, XRD, TGA and electrochemical power capability studies. See DOI: 10.1039/c5ta02043c

diamine and other long chain diamines used, offer an inherent electrochemical dead weight and lead to lower gravimetric specific capacities. Furthermore, Abouimrane *et al.* demonstrated a sodium ion full cell incorporating a disodium terephthalate based organic anode material with traditional transition metal oxide based materials as the cathode.[39] NTCDA derived polyimide based sodium ion full cells have also been demonstrated, but with conventional inorganic materials as cathodes.[35,36] All organic sodium ion full cells with p-doped polymers and organic salt based electrodes have recently been reported, respectively, by Yang *et al.*[40] and Wang *et al.*[32]

Previously, we reported various polyimides derived from 3,4,9,10-perylenetetracarboxylic dianhydride (PTCDA) as electrodes for LIBs with higher reduction potentials and good rate capabilities.[23]

Herein, we report the studies on *N*,*N*′-diamino-3,4,9,10-perylenetetracarboxylic polyimide (PI), based on PTCDA, as a novel cathode material for rechargeable SIBs. The material has been prepared following similar chemistry as in our previous report,[23] with slight modifications to the synthesis protocol. The synthesised PI, with a theoretical capacity of 257 mA h g^{-1} corresponding to a four electron redox process, exhibits good electrochemical activity in the voltage range of 1.5 to 3.5 V *vs.* Na^+/Na, with a reversible capacity of 126 mA h g^{-1}, and with good rate capability. Furthermore, an all-organic sodium ion full cell based on polyimides is demonstrated for the first time, using disodium terephthalate (NaTP) as the anode material and the synthesized PI as the cathode. The full cell exhibits an average discharge voltage of 1.35 V.

2. Experimental section

2.1 Materials synthesis

PI was synthesized by modifying a protocol (Scheme 1) we reported elsewhere.[23] Equimolar PTCDA (1 g, 2.55 mmol) and hydrazine monohydrate (127.5 mg, 2.55 mmol) reacted under reflux conditions in an *N*-methyl-2-pyrrolidone solvent (50 ml) for 6 h under an inert atmosphere. The residue was filtered, washed with ethanol and dried at 120 °C in a vacuum for 12 h. *N*,*N*′-Diamino-3,4,9,10-perylenetetracarboxylic polyimide is also synthesised in an imidazole medium as reported earlier and this will be referred as PI-IMI hereafter. Briefly, a mixture of 2 mmol of 3,4,9,10-perylenetetracarboxylic dianhydride (PTCDA), 2 mmol of diamine, 5.0 g of imidazole and 2 mmol of zinc acetate was heated with stirring at 140 °C for 5 h. The mixture was cooled and poured into 1 N hydrochloric acid. The precipitate was collected through vacuum filtration and washed with boiling saturated potassium carbonate solution followed by distilled water. The product is dried in air at 100 °C. The model derivative PTCDA was used as purchased from Sigma Aldrich. The molten state synthesis technique with imidazole as the solvent involves extensive washing procedures and also results in particles of several microns of size. A solution based synthesis with *N*-methyl-2-pyrrolidone was thus preferred to this molten state synthesis technique.

NaTP was synthesized following a recrystallization method reported by Park *et al.*[29] Briefly, terephthalic acid (1.5 g, 9.04 mmol) was added to a solution of sodium hydroxide (0.91 g, 22.6 mmol) in deionized water (DI water, 5 ml) at 60 °C. DI water was gradually added to the solution at 90 °C until the solution started to show precipitation. After refluxing at 90 °C for 12 h, the crystal was hot-filtered and then dried in a vacuum at 120 °C for 2 h.

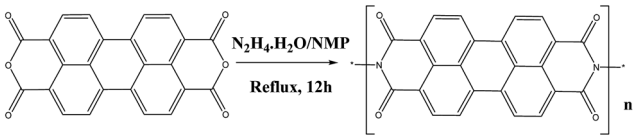

Scheme 1 Schematic diagram for the synthesis of PI.

2.2 Materials characterization

Fourier transform infrared spectra were recorded on a Shimadzu IR Prestige-21 FT-IR spectrometer with KBr pellets. CHNS analysis was carried out on an Elementary vario MICRO cube elemental analyser. Powder X-ray diffraction (XRD) patterns were obtained using an Empyrean, PANanalytical instrument with reference radiation of Cu Kα = 1.540 Å in the range of 5–80°. Solid-state ^{13}C MAS NMR measurement was performed on a Bruker Avance 400 (400 MHz) spectrometer with a MAS rate of 5 kHz. ^1H NMR measurement was performed on a Bruker Avance 500 (500 MHz) spectrometer. Scanning electron microscopy (SEM) images were recorded on a Nova NanoSEM450 FEI scanning electron microscope working at variable voltages from 10 to 30 kV. Thermogravimetric analysis (TGA) was performed using a SDT Q600 Thermogravimetric analyser (TA Instruments). All the electrochemical characterization was carried out using a Biologic SAS VMP3 electrochemical workstation. Porosity characteristics of the samples were studied using N_2 adsorption–desorption isotherms measured at 77 K up to a maximum relative pressure of 1 bar, with the Micrometrics 3-Flex surface characterization analyser.

2.3 Electrochemical measurements

The PI based electrodes were fabricated by mixing an active material, acetylene black and polyvinylidene fluoride (PVDF) in *N*-methyl-2-pyrrolidone (NMP) at a weight ratio of 60 : 30 : 10. The slurry was casted uniformly on stainless steel discs and the electrodes were dried at 65 °C in air for 6 h prior to 12 h drying at 120 °C in a vacuum. A similar procedure was adopted for NaTP electrodes with an active material, acetylene black and PVDF weight ratio of 50 : 37.5 : 12.5. Galvanostatic charge and discharge measurements on the fabricated electrodes were performed in a CR 2032 type coin cell assembled in an argon filled glove box with the moisture and oxygen level maintained at less than 0.1 ppm. 1 M $NaPF_6$ in propylene carbonate was used as the electrolyte in all the electrochemical measurements. Half-cell measurements were done using Na metal as reference and counter electrodes. Full cell measurements were performed by using electrochemically sodiated NaTP as the anode and PI as the cathode. The typical electrode mass loading of the active material is 1.4 mg cm^{-2}.

3. Results and discussion

3.1 Structural and electrochemical characterization of PI

Fig. 1a shows broad FT-IR absorption peaks at 1774 cm^{-1} and 1720 cm^{-1} for PTCDA and two sharp peaks at around 1701 cm^{-1} and 1662 cm^{-1} for PI which correspond to the carbonyl (C=O) asymmetric and stretching frequencies, respectively. The shifts in the carbonyl stretching frequencies suggest the conversion of the anhydride functionality to the imide functionality and the values match with the previous report.[23] The phase purity of PI is confirmed from a comparison with the powder XRD patterns of PI-IMI reported earlier (Fig. 1b).[23] Though both patterns exhibit same 2θ values, it is interesting to look at the peak broadening in the case of PI compared to PI-IMI, which could be due to the reduced particle size as observed in the SEM image (Fig. 1c and d). The modified synthesis procedure results in the formation of PI nanorods of ~100 nm diameter (Fig. 1c), while PI-IMI nanorods were of ~500 nm in diameter (Fig. 1d). Formation of polyimides is further confirmed using solid state ^{13}C MAS NMR spectra and CHNS elemental analysis (see Characterization section, ESI†). PI showed enhanced thermal stability compared to PTCDA as revealed from the TGA analysis (Fig. S1†).[41]

Electrochemical performance of PI was studied by galvanostatic charge–discharge and cyclic voltammetry (CV) studies. CV was carried out to test the reversible ingress of sodium ions into the PI by scanning the potential between 1.5 and 3.5 V *vs.* Na^+/Na at a scan rate of 0.02 mV s^{-1} (Fig. 2a). A pair of reduction peaks at 2.45 and 1.86 V and a pair of oxidation peaks at 2.75 and 1.97 V were observed in the first cycle. The peaks are sharp and have similar intensities, areas and remain almost unchanged in the subsequent cycles. It is clear from the CV that both the oxidation and reduction processes have two continuous steps, which are possibly the formation of the radical anion (PI^-) and radical dianion (PI^{2-}), respectively.[42] The peak positions in the CV are quite consistent with the galvanostatic charge–discharge voltage profiles (Fig. 2b) which showed voltage plateaus around 2.45 and 1.86 V in the discharge profile. The galvanostatic charge–discharge cycling was performed at a high current density of 100 mA g^{-1} in the voltage range of 1.5 to 3.5 V *vs.* Na^+/Na. An initial discharge capacity of 126 mA h g^{-1} was obtained and a capacity retention of ~90% was maintained after 50 cycles of galvanostatic charge–discharge (Fig. 2c). All the charge–discharge curves showed similar features with ~97% columbic efficiency throughout the cycling. The excellent capacity retention upon cycling is attributed to the insolubility of PI in the electrolyte and the high structural stability of the electrode. Hydrazine being the smallest possible diamine, contributes minimally to the electrochemical dead weight of the system in comparison with ethylene, propylene or other long chain diamines.[38] Thus, we observe higher specific capacities with PI. To study the rate capability of the electrode, charge–discharge cycling was performed at current densities ranging from 25 to 800 mA g^{-1} (Fig. 2d). A remarkable 75% capacity retention was observed at 800 mA g^{-1} compared to the specific discharge capacity at 25 mA g^{-1}. The polymerization of the PTCDA by hydrazine, as predicted, reduces dissolution of the active material into the electrolyte and also results in the improved kinetics of electron transfer, leading to better rate performances, as observed. Cycling stability at higher current densities of 50, 100, 200 and 400 mA g^{-1} is also studied (Fig. 2e). A reversible specific discharge capacity of 80 mA h g^{-1} was observed at a high current density of 400 mA g^{-1} after 50 cycles. With a high energy density of 181 W h kg^{-1} at a power density of

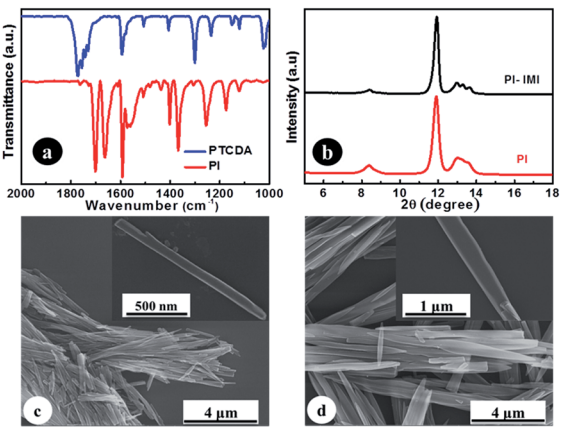

Fig. 1 (a) FT-IR spectra of PTCDA and PI (KBr pellets), (b) powder X-ray diffraction patterns of PI synthesised in *N*-methyl-2-pyrrolidone (PI) and in imidazole (PI-IMI), and SEM micrographs of (c) PI and (d) PI-IMI, the inset showing the respective high-resolution SEM images.

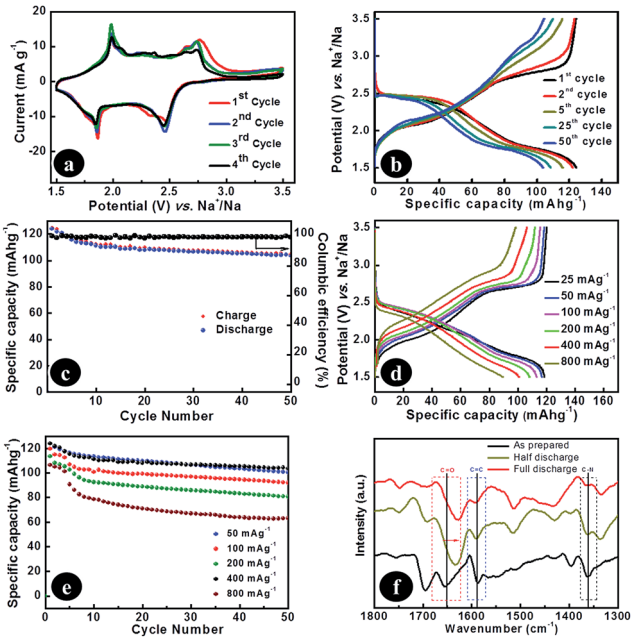

Fig. 2 (a) Cyclic voltammogram of PI scanned within 1.5 to 3.5 V *vs.* Na^+/Na at a scan rate 0.02 mV s^{-1} (b) voltage profile of PI cycled at a current density of 100 mA g^{-1} in a voltage range of 1.5 to 3.5 V *vs.* Na^+/Na (c) charge discharge cycling performance of PI galvanostatically cycled between 1.5 and 3.5 V *vs.* Na^+/Na at a current density of 100 mA g^{-1} and (d) charge–discharge capacities of PI at different current densities; (e) charge–discharge cycling performance of PI galvanostatically cycled between 1.5 and 3.5 V *vs.* Na^+/Na at different current densities and (f) FT-IR spectra for PI at different depths of discharge.

1624 W kg^{-1}, PI based electrodes exhibited excellent electrochemical properties, superior to recently reported polyimides and PTCDA based electrodes for SIBs.[33,35,38] A comparison of energy and power densities of PI with the reported polyimides is illustrated in the Ragone plot (Fig. S2†). The chemical changes in the polyimide during the electrochemical events were investigated using FT-IR spectra (Fig. 2f). The spectra for the fabricated electrodes were taken at 3 different DODs *viz.*, 0% (3.0 V), 50% (2.25 V) and 100% (1.5 V) of the first cycle. The absorbance signals at 1590 and 1359 cm^{-1} from the C=C stretching vibration in the perylene ring and the C–N stretching vibration of imide, respectively, are unchanged, indicating that the carbon–carbon double bonds of the perylene core and carbon–nitrogen single bonds of the imide functionality remain intact during the electrochemical processes. Two sharp peaks at around 1698 and 1653 cm^{-1}, which correspond to the carbonyl (C=O) asymmetric and stretching frequencies, respectively, are red shifted to a broad peak around 1630 cm^{-1} during galvanostatic discharge. This corresponds to the symmetric and asymmetric stretching of C–O–Na which in turn suggests the formation of an enolate during the discharge. Also, a gradual reduction in the intensity of the peak at 1696 cm^{-1} suggests the conversion of the imide functionality.[38] The obtained results are thus in accordance with the mechanism of reversible insertion/deinsertion of sodium ions through enolate formation (Scheme 2). The nanorod morphology with smaller dimensions offers reduced ion diffusion path lengths, which in turn result in good electrochemical performance even at higher current rates. This was further demonstrated by comparing the galvanostatic discharge profiles of PI and PI-IMI by discharging the electrodes at a slow rate of 10 mA g^{-1}. PI showed a smoother and extended flat region with a discharge potential, 100 mV higher than PI-IMI (Fig. S3a†). This can be attributed to the reduced ohmic resistance of the PI based electrodes. The modified synthesis route for polymerization facilitates the formation of this nanorod morphology with smaller dimensions. In addition, N_2 adsorption–desorption isotherms and BET surface area analyses showed improved porosity characteristics for PI compared to PI-IMI (Fig. S3b†). Though both the materials are meso-macro porous in nature, PI exhibits a BET surface area of 102 m^2 g^{-1} compared to that of 41 m^2 g^{-1} for PI-IMI. The enhanced cyclic stability of the PI electrode compared to the PI-IMI electrode (Fig. S3c†) could be attributed to the structural stability of PI upon galvanostatic cycling. To further confirm this, an *ex situ* SEM analysis of the fabricated PI electrodes before galvanostatic cycling (Fig. S4a†) and after 50 cycles of galvanostatic cycling at a current density of 100 mA g^{-1} (Fig. S4b†) was performed. PI nanorods retain their nanorod morphology even after 50 cycles of galvanostatic charge and discharge. This reinforces the concept of polymerisation as an excellent strategy to prevent the electrode dissolution and to impart better mechanical properties for organic electrode materials. Encouraged by the good electrochemical performance of PI, we chose to use this material as the cathode to fabricate an all-organic full cell.

3.2 Electrochemical characterization of a PI-based all-organic full cell

An all-organic full cell is constructed using PI as the cathode material and disodium terephthalate (NaTP) as the anode material. As-synthesized NaTP was well characterized using FT-IR, XRD and ^{1}H NMR. An FT-IR spectrum for as-synthesised NaTP shows sharp peaks at 1551 cm^{-1} and 1380 cm^{-1}, which correspond to carboxylate asymmetric and symmetric stretching frequencies, respectively, (Fig. S5a†). Also, the disappearance of the broad peak around 3300–3600 cm^{-1} corresponds to O–H stretching and the broad carbonyl stretching band at 1671 cm^{-1} suggests the formation of the salt. Formation of NaTP is confirmed using ^{1}H NMR spectra (see Characterization section, ESI†). Furthermore, thermogravimetric analysis shows no weight loss in the sample around 320 °C, which suggests an absence of terephthalic acid monosodium salt (Fig. S5b†). The phase purity of as-synthesised NaTP is confirmed using the powder X-ray diffraction technique and the pattern matches with the ICDD reference number 00-052-2146 (Fig. S6†).

Terephthalic acid disodium salt has previously been demonstrated as a promising anode material with a two sodium redox insertion process for sodium ion batteries (Scheme 3).[29] Fig. 3a shows the cyclic voltammogram for the NaTP electrode scanned in the voltage range of 0 to 2 V at a scan rate of 0.02 mV s^{-1} *vs.* Na^+/Na. Fig. 3b shows the galvanostatic charge–discharge voltage curve for NaTP cycled with a current density of 50 mA g^{-1} in the voltage range of 0 to 2 V. A perfect coherence is observed between the redox peaks observed at 0.25 V at 0.05 V in the CV and voltage plateaus observed in the galvanostatic charge–discharge profiles.

The peak at 0.25 V corresponds to the enolate formation of terephthalic carboxylate salt and the peak at 0.05 V corresponds to sodium ion insertion into the conductive carbon additive.[29] A stable specific discharge capacity of around 180 mA h g^{-1} was obtained during the cycling. NaTP was thus chosen as the anode for the fabrication of an all-organic sodium ion full cell.

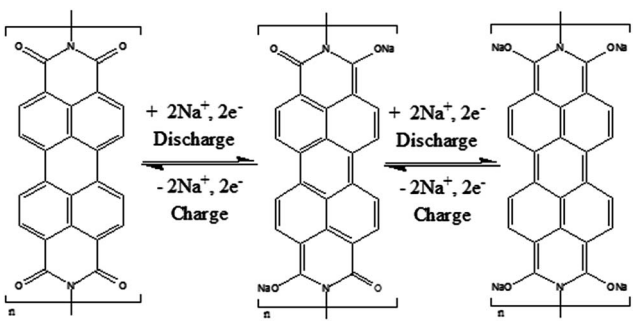

Scheme 2 Schematic representation of the charge–discharge mechanism for PI.

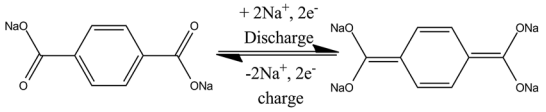

Scheme 3 Schematic representation of the charge–discharge mechanism for NaTP.

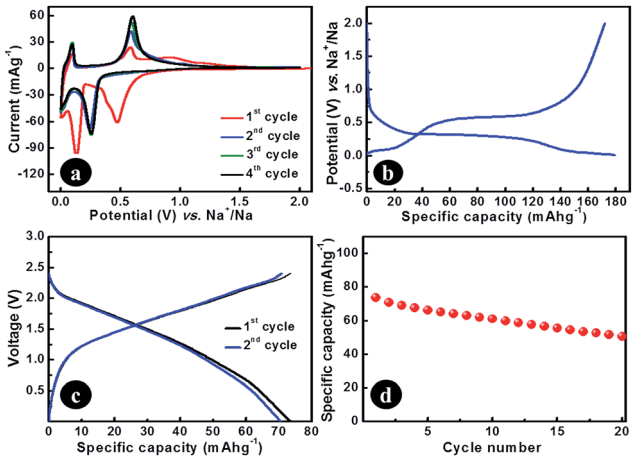

Fig. 3 (a) Cyclic voltammogram of NaTP scanned within 0 to 2 V *vs.* Na^+/Na at a scan rate of 0.02 mV s^{-1} and (b) voltage profile of NaTP cycled at a current density of 50 mA g^{-1} in a voltage range of 0 to 2 V *vs.* Na^+/Na; (c) voltage profile of PI-NaTP full-cell galvanostatically cycled at a current density of 50 mA g^{-1} in a voltage range of 0 to 2.4 V; (d) cycling performance of PI-NaTP full-cell galvanostatically cycled at a current density of 50 mA g^{-1} in a voltage range of 0 to 2.4 V. Specific capacity is calculated based on the mass of both anode and cathode active materials.

An all-organic sodium ion full cell using polyimide as the cathode was realized for the first time by coupling it with electrochemically sodiated NaTP, as the anode. Electrochemical sodiation was done by discharging the NaTP electrode to full capacity (0.1 V *vs.* Na^+/Na) in a half cell configuration with a current density of 50 mA g^{-1}. Based on the stable specific discharge capacities obtained for the two electrodes, cathode and anode materials with an optimized weight ratio of 1.6 : 1 was used to fabricate the full cell. The coin cells were galvanostatically cycled in the voltage window of 0 to 2.4 V at a current density of 50 mA g^{-1} (Fig. 3c and d). The specific capacities of the full cell are calculated based on the active material weights of both the anode and cathode. The fabricated full cell exhibits an average discharge potential of 1.35 V with an initial specific capacity of 73 mA h g^{-1} (Fig. 3c), which is almost double the initial discharge capacity of 40 mA g^{-1} observed for the full cell fabricated with NTCDA based polyimide as the anode.[36] A gradual decrease in the specific capacity upon cycling was observed (Fig. 3d), which could be improved with further optimization of the electrode loading and other cell parameters.

4. Conclusions

To summarize, for the first time, we have demonstrated an all-organic sodium ion full cell using PTCDA based polyimide and disodium terephthalate (pre-sodiated) redox active molecules as the cathode and the anode, respectively. The as-synthesized PI exhibited excellent electrochemical performance, when studied as a cathode for a rechargeable sodium battery, with a maximum energy density of 254 W h kg^{-1} and a maximum power density of 1624 W kg^{-1} when cycled against Na. While the half-cell measurements on the PI electrode showed a stable reversible capacity of 126 mA h g^{-1} with good capacity retention and rate capability, the all-organic sodium ion full cell delivered an initial capacity of 73 mA h g^{-1}. The excellent electrochemical performance of the polyimide material is attributed to the insolubility of the electrode in the electrolyte and its high structural stability. With the obtained attractive performances of the PTCDA-based PI material, we believe that the present study will lead to new directions to tailor the organic materials for their applications in SIBs.

Acknowledgements

H.B. acknowledges INSPIRE fellowship, Department of Science and Technology (DST), Govt. of India. D.D. and K.N acknowledge CSIR, Govt. of India, for financial support. M.H. acknowledges the Science and Engineering Research Board, SERB/F/0962, for the partial financial support of this work. M.M.S. acknowledges the Department of Biotechnology (DBT), Govt. of India, for financial support of this work through DBT's Twinning programme for the NE (BT/350/NE/TBP/2012).

Notes and references

1 S.-W. Kim, D.-H. Seo, X. Ma, G. Ceder and K. Kang, *Adv. Energy Mater.*, 2012, **2**, 710.
2 H. Pan, Y.-S. Hu and L. Chen, *Energy Environ. Sci.*, 2013, **6**, 2338.
3 V. Palomares, P. Serras, I. Villaluenga, K. B. Hueso, J. Carretero-Gonzalez and T. Rojo, *Energy Environ. Sci.*, 2012, **5**, 5884.
4 Y. Cao, L. Xiao, W. Wang, D. Choi, Z. Nie, J. Yu, L. V. Saraf, Z. Yang and J. Liu, *Adv. Mater.*, 2011, **23**, 3155.
5 N. Yabuuchi, M. Kajiyama, J. Iwatate, H. Nishikawa, S. Hitomi, R. Okuyama, R. Usui, Y. Yamada and S. Komaba, *Nat. Mater.*, 2012, **11**, 512.
6 Z. Jian, W. Han, X. Lu, H. Yang, Y.-S. Hu, J. Zhou, Z. Zhou, J. Li, W. Chen, D. Chen and L. Chen, *Adv. Energy Mater.*, 2013, **3**, 156.
7 C. S. Park, H. Kim, R. A. Shakoor, E. Yang, S. Y. Lim, R. Kahraman, Y. Jung and J. W. Choi, *J. Am. Chem. Soc.*, 2013, **135**, 2787.
8 J. Qian, M. Zhou, Y. Cao, X. Ai and H. Yang, *Adv. Energy Mater.*, 2012, **2**, 410.
9 M. Armand and J. M. Tarascon, *Nature*, 2008, **451**, 652.
10 H. Chen, M. Armand, G. Demailly, F. Dolhem, P. Poizot and J.-M. Tarascon, *ChemSusChem*, 2008, **1**, 348.
11 J.-M. Tarascon, *ChemSusChem*, 2008, **1**, 777.
12 C. Luo, R. Huang, R. Kevorkyants, M. Pavanello, H. He and C. Wang, *Nano Lett.*, 2014, **14**, 1596.
13 Y. Morita, S. Nishida, T. Murata, M. Moriguchi, A. Ueda, M. Satoh, K. Arifuku, K. Sato and T. Takui, *Nat. Mater.*, 2011, **10**, 947.
14 Y. Liang, P. Zhang and J. Chen, *Chem. Sci.*, 2013, **4**, 1330.
15 H. Chen, M. Armand, M. Courty, M. Jiang, C. P. Grey, F. Dolhem, J.-M. Tarascon and P. Poizot, *J. Am. Chem. Soc.*, 2009, **131**, 8984.

16 K. Sakaushi, G. Nickerl, F. M. Wisser, D. Nishio-Hamane, E. Hosono, H. Zhou, S. Kaskel and J. Eckert, *Angew. Chem., Int. Ed.*, 2012, **51**, 7850.
17 Z. Song, H. Zhan and Y. Zhou, *Angew. Chem., Int. Ed.*, 2010, **49**, 8444.
18 Y. Liang, P. Zhang, S. Yang, Z. Tao and J. Chen, *Adv. Energy Mater.*, 2013, **3**, 600.
19 M. Armand, S. Grugeon, H. Vezin, S. Laruelle, P. Ribiere, P. Poizot and J. M. Tarascon, *Nat. Mater.*, 2009, **8**, 120.
20 S. Wang, L. Wang, K. Zhang, Z. Zhu, Z. Tao and J. Chen, *Nano Lett.*, 2013, **13**, 4404.
21 Z. Song, Y. Qian, X. Liu, T. Zhang, Y. Zhu, H. Yu, M. Otani and H. Zhou, *Energy Environ. Sci.*, 2014, **7**, 4077.
22 Y. Liang, Z. Tao and J. Chen, *Adv. Energy Mater.*, 2012, **2**, 742.
23 P. Sharma, D. Damien, K. Nagarajan, M. M. Shaijumon and M. Hariharan, *J. Phys. Chem. Lett.*, 2013, **4**, 3192.
24 X. Han, C. Chang, L. Yuan, T. Sun and J. Sun, *Adv. Mater.*, 2007, **19**, 1616.
25 Z. Song, H. Zhan and Y. Zhou, *Chem. Commun.*, 2009, **4**, 448.
26 B. Genorio, K. Pirnat, R. Cerc-Korosec, R. Dominko and M. Gaberscek, *Angew. Chem., Int. Ed.*, 2010, **49**, 7222.
27 Y. Hanyu and I. Honma, *Sci. Rep.*, 2012, **2**, 453.
28 T. Nokami, T. Matsuo, Y. Inatomi, N. Hojo, T. Tsukagoshi, H. Yoshizawa, A. Shimizu, H. Kuramoto, K. Komae, H. Tsuyama and J.-i. Yoshida, *J. Am. Chem. Soc.*, 2012, **134**, 19694.
29 Y. Park, D.-S. Shin, S. H. Woo, N. S. Choi, K. H. Shin, S. M. Oh, K. T. Lee and S. Y. Hong, *Adv. Mater.*, 2012, **24**, 3562.
30 K. Sakaushi, E. Hosono, G. Nickerl, T. Gemming, H. Zhou, S. Kaskel and J. Eckert, *Nat. Commun.*, 2013, **4**, 1485.
31 K. Chihara, N. Chujo, A. Kitajou and S. Okada, *Electrochim. Acta*, 2013, **110**, 240.
32 S. Wang, L. Wang, Z. Zhu, Z. Hu, Q. Zhao and J. Chen, *Angew. Chem., Int. Ed.*, 2014, **53**, 5892.
33 W. Luo, M. Allen, V. Raju and X. Ji, *Adv. Energy Mater.*, 2014, **4**, 1400554.
34 C. Luo, Y. Zhu, Y. Xu, Y. Liu, T. Gao, J. Wang and C. Wang, *J. Power Sources*, 2014, **250**, 372.
35 L. Chen, W. Li, Y. Wang, C. Wang and Y. Xia, *RSC Adv.*, 2014, **4**, 25369.
36 H. Qin, Z. P. Song, H. Zhan and Y. H. Zhou, *J. Power Sources*, 2014, **249**, 367.
37 M. Andrzejak, G. Mazur and P. Petelenz, *J. Mol. Struct.*, 2000, **527**, 91.
38 H.-g. Wang, S. Yuan, D.-l. Ma, X.-l. Huang, F.-l. Meng and X.-b. Zhang, *Adv. Energy Mater.*, 2014, **4**, 1301651.
39 A. Abouimrane, W. Weng, H. Eltayeb, Y. Cui, J. Niklas, O. Poluektov and K. Amine, *Energy Environ. Sci.*, 2012, **5**, 9632.
40 W. Deng, X. Liang, X. Wu, J. Qian, Y. Cao, X. Ai, J. Feng and H. Yang, *Sci. Rep.*, 2013, **3**, 2671.
41 M. Ghosh and K. Mittal, *Polyimides: Fundamentals and Applications*, Marcel Dekker, New York, 1996.
42 C. De Luca, C. Giomini and L. Rampazzo, *J. Electroanal. Chem.*, 1990, **280**, 145.